Journal of Sedimentary Research

Journal of Sedimentary Research, 2016, v. 86, 1328–1343
Research Article
DOI: http://dx.doi.org/10.2110/jsr.2016.79

TRAVERTINES ASSOCIATED WITH HYPERALKALINE SPRINGS: EVALUATION AS A PROXY FOR PALEOENVIRONMENTAL CONDITIONS AND SEQUESTRATION OF ATMOSPHERIC CO_2

THOMAS LELEU,[1] VALERIE CHAVAGNAC,[1] ADELIE DELACOUR,[1,2] CATHERINE NOIRIEL,[1] GEORGES CEULENEER,[1] MARKUS ARETZ,[1] CELINE ROMMEVAUX,[3] AND SANDRA VENTALON[4]

[1] *Géosciences Environnement Toulouse, Observatoire Midi-Pyrénées, Université de Toulouse, CNRS, IRD, Université Paul Sabatier, 14 Avenue Edouard Belin, 31400 Toulouse, France*

[2] *Université de Lyon, UJM-Saint-Etienne, Laboratoire Magmas et Volcans, UMR 6524, F-42023 Saint Etienne, France*

[3] *Laboratoire Géomicrobiologie, CNRS, IPGP, Sorbonne Paris Cité, Université Paris Diderot, UMR 7154, Paris, France*

[4] *Université de Lille 1, CNRS, UMR 8187 LOG, 59655 Villeneuve d'Ascq, France*

e-mail: thomas.leleu@get.obs-mip.fr

ABSTRACT: **Travertine are found in ophiolite massifs in association with bicarbonate-depleted hyperalkaline spring waters (pH up to 11.9), in contrast with most continental carbonates (e.g., travertine, tufa, speleothems) that precipitate from calcium bicarbonate-enriched waters. Here travertines formed from bicarbonate-depleted hyperalkaline spring water were subjected to a multidisciplinary and multi-scale approach to evaluate their potential as proxies of past climatic records and sequestration of atmospheric CO_2.**

Two mechanisms of calcium carbonate precipitation were apparent: 1) hydration-hydroxylation reaction due to the mixing of hyperalkaline and surface runoff waters, or 2) dissolution of atmospheric $CO_{2(g)}$ into hyperalkaline waters.

For two sites, the bulk chemical signature of travertines (Mg, Ca, and Sr wt%) are consistent with "prior calcite precipitation" (PCP) processes and thus likely records the environmental conditions at the time of their formation. However, for the third site, the trace-element concentrations in the various carbonate fabrics indicate some recrystallization. Constant $\delta^{18}O$ values indicate that hydration and hydroxylation reactions completely buffer the oxygen isotope composition of the water (equilibrium state) from which a paleo-temperature can be estimated. In contrast, $\delta^{13}C$ values reflect potential carbon sources, either from surface runoff waters or atmospheric CO_2.

Within the framework of continental carbonate, calcium carbonate formation in bicarbonate-depleted hyperalkaline environments results in a linear and positive co-variation of $\delta^{18}O$ and $\delta^{13}C$ values and defines a unique and distinctive stable-isotope field on a $\delta^{18}O$–$\delta^{13}C$ plot, in contrast to carbonates formed in more typical bicarbonate-enriched environments. Moreover, the combined variations in $\delta^{18}O$, $\delta^{13}C$, and $^{87}Sr/^{86}Sr$ between laminae document the changes in the paleo-activity of hyperalkaline spring and surface runoff waters on the time scale of formation. The $^{87}Sr/^{86}Sr$ ratio represents a tracer for quantifying surface runoff water contribution. Furthermore, the amount of CO_2 sequestrated in travertine has been estimated following different scenarios of formation. The calculated CO_2 sequestrated for these deposits ranges from 9 $kgCO_2\ yr^{-1}$ to 522 $kgCO_2\ yr^{-1}$.

INTRODUCTION

Continental carbonates (e.g., speleothems, calcrete, lacustrine limestone, travertine, calcareous tufa, and tufa) are characterized by specific petrofacies resulting from a complex and dynamic interplay of physical, chemical, and biological activity (e.g., Pentecost 2005 and reference therein; Fouke 2011; Gandin and Capezzuoli 2014; Arenas et al. 2014; Capezzuoli et al. 2014). The characterization of continental carbonate is of growing interest because of their ability to preserve paleoenvironmental and paleoclimate information at the time of their formation.

Overall, continental carbonates form predominantly at ambient temperature from calcium bicarbonate–enriched ($Ca\text{-}CO_3^{2-}$ type) waters. Alkalinity is derived either from dissolution of carbonate minerals, CO_2 present in the atmosphere and soils above water table, or CO_2 thermally generated in the deep Earth's crust (Pentecost and Viles 1994; Pentecost 2005).

Alternatively, continental carbonates can be associated with hyperalkaline thermal springs located in ophiolite massifs, where circulating groundwaters interact with deep crustal rock and are typically depleted in dissolved inorganic carbon (DIC, e.g., Oman: Neal and Stanger 1983, Chavagnac et al. 2013a; New Caledonia: Launay and Fontes 1985, Monnin et al. 2014; Philippines: Abrajano et al. 1988). In this case, the serpentinization process has led to the conversion of initial $Mg\text{-}HCO_3$ type waters into Ca-OH type hyperalkaline waters depleted both in DIC and Mg but enriched in Ca (Barnes et al. 1967; Barnes and O'Neil 1969; Barnes et al. 1978; Neal and Stanger 1984; Bruni et al. 2002; Cipolli et al. 2004; Sader et al. 2007; Kelemen and Matter 2008; Chavagnac et al. 2013b; Monnin et al. 2014). Precipitation of calcium carbonate from hyperalkaline spring waters is possible only if carbonate ions are available which is typically accomplished in two ways: 1) mixing between DIC-depleted hyperalkaline waters and DIC-rich surface runoff waters, and/or

Published Online: November 2016
 1527-1404/16/086-1328/$03.00

2) via diffusion and dissolution of atmospheric $CO_{2(g)}$ into spring waters. As a result, the conditions leading to calcium carbonate formation in hyperalkaline springs is fundamentally different from carbonates that precipitate from bicarbonate-rich waters. However, thus far little is known on the reliability of these deposits as a proxy for past climatic records.

The purpose of this study is to provide a comprehensive and detailed study of three calcium carbonate deposits formed at DIC-depleted hyperalkaline springs in the Oman ophiolite. The objectives are 1) to assess the relationship between the petrologic features and fabrics and the geochemical and isotopic signatures, and 2) to discuss the potential of these deposits as proxies for the past climatic record and sequestration of atmospheric CO_2.

BACKGROUND

General Spring Characteristics and Nomenclature

The general characteristics of carbonate deposits collected in Oman can be summarized as follows:

1) They are associated with warm-temperature (20–65°C) hyperalkaline springs (pH ranges from 10 to 11.9) extremely depleted in Mg and DIC; the springs are preferentially located near two major structural discontinuities, i.e., the basal thrust plane (the contact between the peridotitic mantle section and the underlying sedimentary and metamorphic rocks) and the "paleo-Moho" (the contact between the peridotite mantle section and the overlying gabbroic crustal section) (Neal and Stanger 1984; Pauckert et al. 2012; Chavagnac et al. 2013a).
2) Gas emissions at these springs are essentially composed of $H_{2(g)}$ and $CH_{4(g)}$ without any $CO_{2(g)}$ (Sano et al. 1993; Boulart et al. 2013).
3) Mineral assemblage forming at spring discharge is essentially composed of calcite and aragonite (Chavagnac et al. 2013b).
4) Climatic conditions, e.g., arid or wet seasons, influence the formation rates and the morphologies of the carbonate deposits (Clark and Fontes 1990; Clark et al. 1992).

Over the last 20 years, classification and definition of continental carbonates have evolved based on lithological, petrological, geochemical, and isotopic characteristics (e.g., Capezzuoli et al. 2014; Gandin and Capezzuoli 2008; Pentecost 2005; Ford and Pedley 1996; Pentecost and Viles 1994).

Based on the most recent classification of Capezzuoli et al. (2014), the Oman carbonate deposits share characteristics that are indicative of both travertine and tufa deposits, i.e., "calcareous tufa" or "travitufa." However, their formation is directly linked to the activity of hyperalkaline waters, which testifies to a hydrothermal origin, i.e., a closer link to travertine terminology. Therefore, we refer to these deposits as travertine in agreement with previous publications (Clark and Fontes 1990; Clark et al. 1992; Mervine et al. 2014).

Geological Context

The Oman ophiolite is one of the largest and best-preserved sections of oceanic lithosphere (30,000 km^2) exposed on land (Coleman 1981), (Fig. 1). The ophiolite is composed of two major lithological units, the mantle section and the crustal section. The mantle section rests on top of a metamorphic, amphibolitic sole, itself resting on sedimentary rocks (carbonates, sandstones, and radiolarites) (e.g., Coleman 1981). It is formed mostly by variably serpentinized residual mantle harzburgites and dunites. Mafic to felsic intrusive lithologies (pyroxenites, wehrlites, troctolites, gabbros, tonalities) are a minor although ubiquitous constituent of the mantle section (Boudier and Coleman 1981; Ceuleneer et al. 1996; Amri et al. 1996; Python and Ceuleneer 2003). The crustal section, which overlies the mantle section, is more heterogeneous in terms of lithology, including ultramafic and gabbroic cumulates (Juteau et al. 1988; Abily and Ceuleneer 2013), granitic differentiates, and extrusive rocks (diabase dikes and pillow lavas) (Pallister and Hopson 1981; Alabaster et al. 1982; Amri et al. 1996).

At present, alteration of the ultramafic rocks through serpentinization reactions is driven by percolation of ancient and/or modern meteoric waters through fractures (Chavagnac et al. 2013a). Serpentinization reactions lead to the formation of hyperalkaline springs (25 to 40°C, Chavagnac et al. 2013a), which are numerous over the entire ophiolite belt and associated with travertine deposits (Neal and Stanger 1984; Kelemen et al. 2011; Chavagnac et al. 2013a; Mervine et al. 2014) (Figs. 1, 2).

Climate of Oman

The ophiolite crops out in the Northern Oman Mountains, located at the southeastern horn of the Arabian Peninsula (22–24°N). The climatic conditions are typical of a dry tropical area, with maximum air temperature ranging between 20 and 35°C during winter and > 40°C in summer. The climate of the northeastern side of the mountain faces the Gulf of Oman and has some marine influence, whereas the southwestern side faces the Arabian Sands and is predominantly continental. The present-day average rainfall on the Northern Oman Mountains is on the order of 100 mm yr^{-1} (Clark and Fontes 1990) and is influenced by two sources of precipitation: the Mediterranean Sea and the Indian Ocean. These two influences define a boundary called the Inter-Tropical Convergence Zone (ITCZ). The ITCZ varies seasonally along a north to south gradient. The Oman hydrology is highly variable because of the rainfall intensity variation and evaporation rates (Kwarteng et al. 2009).

Paleoclimate Records of Oman

Over longer timescales, paleoclimate studies on various materials (speleothems, lake sediments, and travertine) have revealed an alternation of humid and arid periods in Oman (Clark and Fontes 1990; Clark et al. 1992; Fleitmann et al. 2003; Fleitmann et al. 2004; Fleitmann et al. 2007; Fuchs and Buerkert 2008; Mervine et al. 2014). ^{14}C dating methods, geochemistry, and stable-isotope (C and O) signatures were used to determine the timespan during which precipitation intensity had varied. For example, Fleitmann et al. (2003) linked the temporal $\delta^{18}O$ variations of the precipitation recorded in speleothems (between –12 and –4‰) from Hoti cave (Oman) to the ITCZ shifts. Typically, previous results concentrated their effort on either geochemical features or petrological ones, rather than a combination of the two. Such observations are, however, crucial to elucidate the causal-consequence link between climate change and travertine morphology.

SAMPLES AND METHODS

Among a large series of travertine sites visited during three field campaigns (December 2008, January 2010, and January 2011), three sites were selected from hyperalkaline springs for which geological setting, chemical composition of hyperalkaline spring waters, gas emissions, and mineralogical assemblages have been carefully studied (Neal and Stanger 1984; Weyhenmeyer et al. 2002; Pauckert et al. 2012; Chavagnac et al. 2013a; Chavagnac et al. 2013b; Boulart et al. 2013; Mervine et al. 2014) (Fig. 1, Table 1) and best elucidate the different styles of carbonate precipitation. The samples were sawn with a diamond blade perpendicular to the lamination for microscopic-scale description. In addition, we used a micro-dremel to powder each lamina of samples 32 and 33, which were first identified in microscopic observations (Fig. 3). To decipher whether travertine formed in a DIC-depleted environment constitutes a potential proxy of past climate variability, each sample was consequently characterized using various analytical techniques (details are reported in the Appendix Supplementary Material). We summarize their usefulness below:

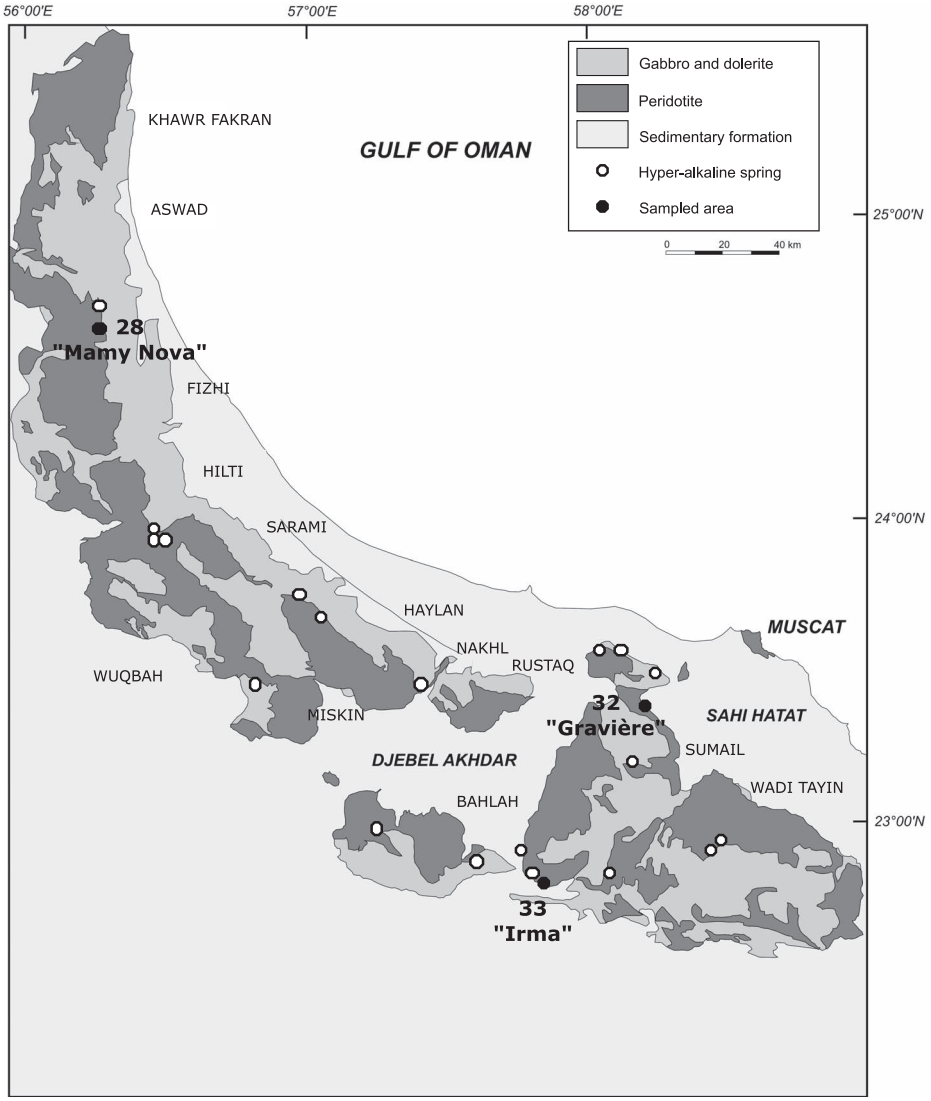

FIG. 1.—Simplified geological map of the Sultanate of Oman (modified from Chavagnac et al. 2013b).

- Scanning electron microscopy (SEM) coupled with energy-dispersive spectroscopy (EDS) to identify chemical changes in the sample, based on code color imaging of chemical elements on thin-section areas.
- Raman analysis and cathodoluminescence in order to determine calcium carbonate polymorphs from thin sections.
- Electron microprobe analyses to detect and observe the repartition of substituted elements into the carbonates, such as magnesium (Mg) and strontium (Sr).
- Oxygen and carbon isotope compositions were conducted to identify precipitation mechanisms and to characterize mixing processes.
- $^{87}Sr/^{86}Sr$ isotope composition in order to quantify the mixing proportion between surface runoff and hyperalkaline spring waters that control the formation of travertine.

RESULTS

Site Description and Petrographic Analysis

In the first section of this paper, we describe each sampling site following the concept of sedimentary depositional facies (Fouke et al. 2001; Veysey et al. 2008; Fouke 2011) together with the main microscopic observations. In the following sections, we present the stable-isotope and radiogenic-isotope compositions from two of the sites.

"Mamy Nova" Site (Sample 28)

Site "Mamy Nova" is located in the wadi Zabyn, running through the Fizh massif (Fig. 1). The local topographic and geological setting corresponds to a mixing area between runoff and groundwaters that interacted with mantle peridotites on their way to the spring, although the main discharge itself lies on a gabbroic substratum. However, no sedimentary and metamorphic rocks are found in wadi Zabyn upstream from spring waters, which run exclusively in the mantle harzburgites. In the valley bottom, terrace deposits composed of cemented gravel bars are partially preserved, topping the gabbroic substratum. Both terrace and substratum are incised by the stream flow. The hyperalkaline spring discharge is located 1 to 2 m above the surface waters and emerges from a fractured zone running through the lower crustal section (Table 1; Fig. 2). Modern to ancient carbonate deposits occur from the spring discharge area over a distance of 1 km along the surface waters. Carbonate encrustation around gravels can be observed in the stream bottom. Small-scale (10 cm high) step-shaped micro-terracettes are present in the channel facies.

FIG. 2.—Photographs of the sampling sites presenting the carbonate depositional facies at the hyperalkaline springs.

Sample 28 was taken from a carbonate gravel bar, which consists of a conglomerate of ultramafic rocks partially cemented by calcium carbonate. Pores are partially filled with detrital material consisting of a mixture of micritic allochems (clotted peloids partially cemented or redissolved), micrite, clays, and ultramafic fragments (Fig. 4A). Precipitation of carbonates occurred in the vadose zone, as suggested by the presence of aragonite microstalactic cement in some pores and discontinuous ≈ 100-µm-thick drusy calcite cement that precipitated around the pores (Fig. 4B, C, D). Si- and Mg-rich clavate (10–25 µm in diameter and rich in organic matter) that underline a growth stage of the drusy isopacheous sparite, as

TABLE 1.—*Location and geological context of travertine samples. Chemical composition of hyperalkaline springs: Chavagnac et al. (2013b); Mineralogical precipitates™: Chavagnac et al. (2013a).*

Site	Name	Latitude (N)	Longitude (E)	Altitude (masl)	Geological Context	T (°C)	pH	Surface Precipitate™	Stream-Bed Precipitate™	Consolidated Precipitate™
28	Mamy Nova	24°31′221	56°18′071	395	Within the crustal section, bedded gabbro and ultrabasic cumulates	38.6	11.0	Aragonite, brucite	Aragonite, brucite	Aragonite, calcite, hydrotalcite? Iowaite?
32	Gravière	23°19′211	58°13′421	367	Mixing peridotite gabbro, very altered	31.0	11.5	Calcite, aragonite	Aragonite, brucite, suolunite	Aragonite, calcite, hydrotalcite?
33	Irma	22°48′431	57°50′161	485	In serpentinite, just above the contact with Hawasinah	25.8	11.7	Calcite, aragonite	Calcite	Calcite

well as the presence of aragonite needle-like features topped by a Si- and Mg-rich film (Fig. 4B).

"Gravière" Site (Sample 32)

At this site, the substratum of the hyperalkaline spring is located close to the boundary between mantle peridotites and lower crustal gabbroic cumulates. Meteoric waters travel through a large drainage system originating in the sedimentary and metamorphic rocks of the Saih Hatat and running through mantle peridotites (Table 2; Fig. 1). The valley is partially filled with highly cemented gravel bars that are incised by stream flow and partially covered by uncemented modern gravels. The hyperalkaline spring emerges on cemented gravel bars, where it mixes with the surface runoff waters (Fig. 2). At the spring discharge area, a modern carbonate deposit can be observed covering the stream bottom. Sample 32 was taken in the channel facies where the wadi Mansah and the hyperalkaline spring mix (Fig. 2). A green algae and/or bacterial mat covers the modern surface of the carbonate deposit in the channel facies (Fig. 2).

On a macroscopic scale, the sample is composed of a succession of 13 laminae exhibiting distinctive coloration, mineralogy, fabrics, and porosity (Fig. 5). The observations are summarized in Table 2. The sample displays a very complex spatial organization, with an alternation of light-, intermediate-, and dark-gray layers (Fig. 5). The laminae are composed of gothic-arch calcite, crystallized aragonite bushes, drusy calcite cement (Fig. 5, zones A and B), a Mg-, and Si-rich organic material (Fig. 5, zones A, B, D, and E) that contains also Al, dark-gray spheroids (Fig. 5, zone C), and micro-spheroids embedded in Mg-, Al-, and Si-rich organic material (Fig. 5, zone D). Large pores are also filled with drusy calcite cement (Fig. 5, zone C).

"Irma" Site (Sample 33)

The "Irma" site is located along the foothills of the Samail Massif in mantle peridotites overlying the sedimentary rocks of the Hawasina

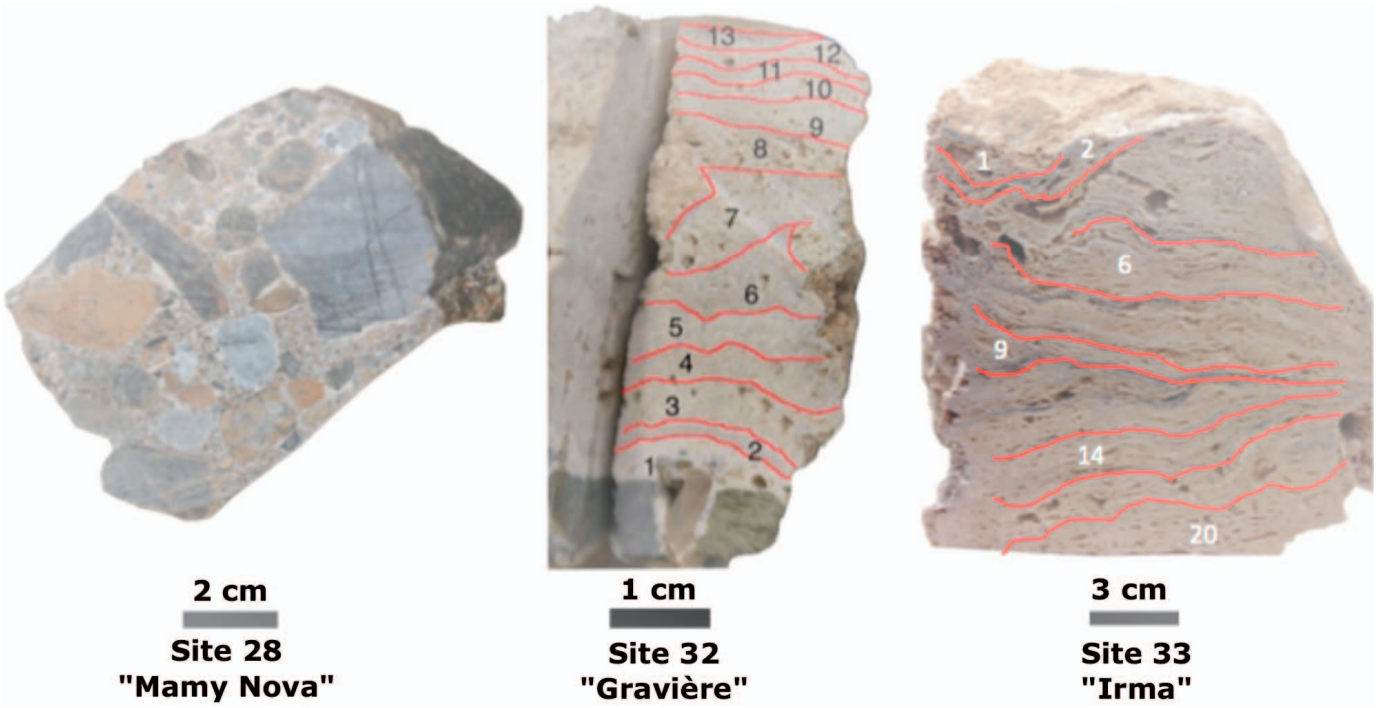

FIG. 3.—Macroscopic photographs of the three studied carbonate samples. On samples 32 and 33 hand specimens, we denote the laminae identified upon microscopic observation.

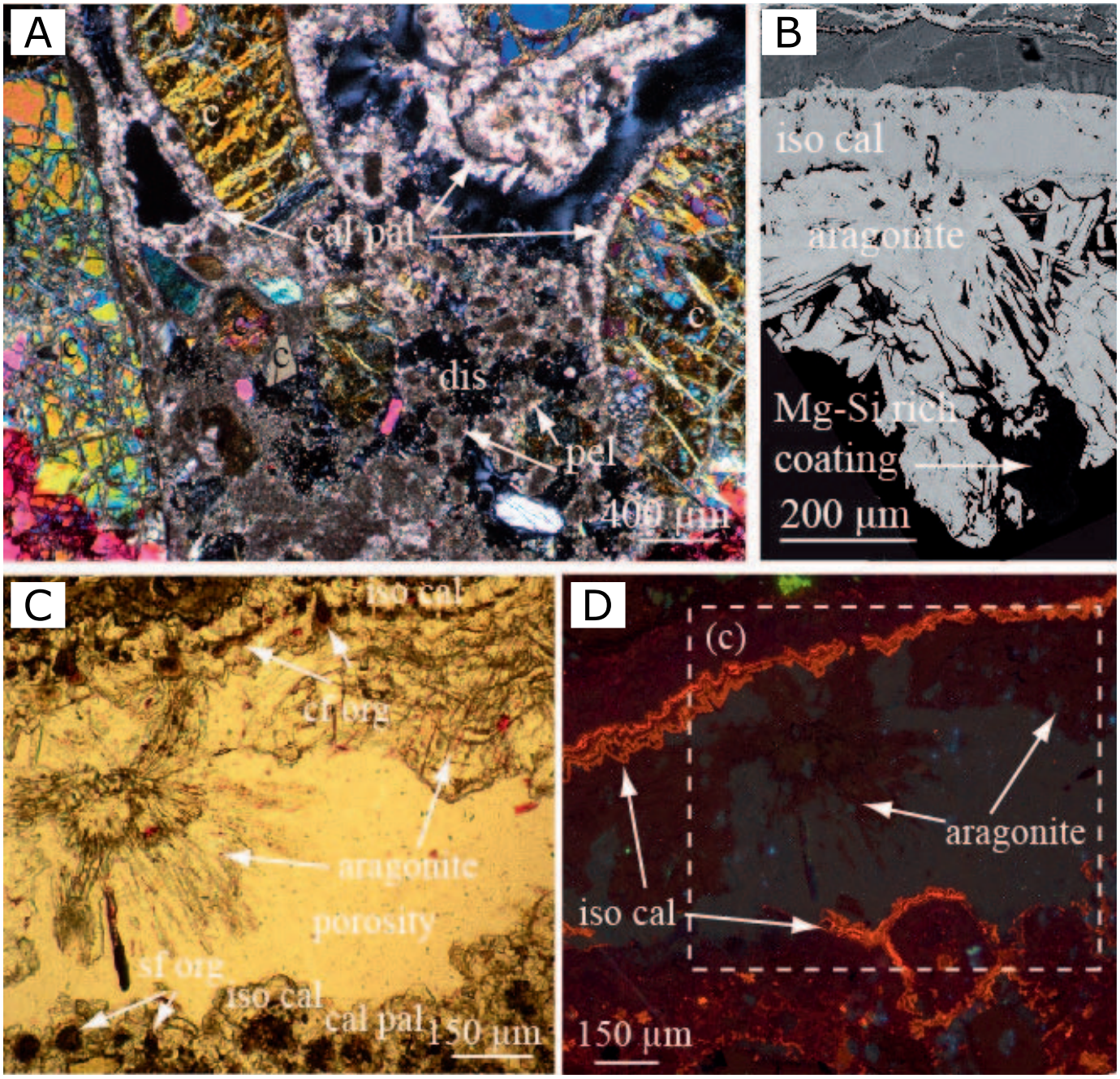

FIG. 4.—Microscopic observations of sample 28 in **A)** plane-polarized light; **B)** SEM-EDX; **C)** detail of a pore which depicts aragonite bush, and both aragonite and calcite cement in transmitted polarized-light microscopy; **D)** view of area **C)** in cathodoluminescence. Legend: pel, peloid; c, ultramafic element of the conglomerate; iso cal, isopachous calcite cement; dis, dissolution feature; sf org, spherical feature (organic material); cf org, clavate feature (organic material); dis, dissolution feature; cal pal, palisade calcite.

Formation and the greenschists and amphibolites of the metamorphic sole (Fig. 1). The local drainage system is located entirely within highly serpentinized mantle peridotites. The site itself is a large kilometer-wide terrace characterized by a layer of recent travertine several meters thick. There is no obvious surface runoff, implying that the precipitation of calcium carbonate takes up carbon from atmospheric CO_2 (Table 2; Fig. 2). Deposits form successive pools separated by aprons around and downstream of the hyperalkaline spring (Fig. 2).

Sample 33 was collected in the flowing hyperalkaline spring. It consists of calcite raft (sparite) deposits alternating with more organic-rich layers of vuggy calcite (micrite) displaying a laminoid-fenestral fabric (type LF-A according to Flügel (2004); Fig. 6A, B). Sparite overgrowths are observed on both sides of the rafts (Fig. 6D). Ultramafic detrital particles may occur between rafts (Fig. 6C).

Chemical Composition of Carbonate Fabrics

Electron microprobe analyses were carried out on the various calcium carbonate fabrics. Chemical compositions of carbonate samples are reported in Table 3 and Figure 7 according to the sample and from

TABLE 2.—*Microscopic description of samples based on petrographic fabrics and mineralogy.*

Travertine Site/Name	Lamina	Petrographic Fabric
28/Mamy Nova	lamina 1: contact with substrate	Fibrous aragonite
	lamina 2: pore filling	Needle-like aragonite
32/Gravière	lamina 1 and 2: contact with substrate	Laminae of recrystallized aragonite bushes and drusy calcite cement
	lamina 3 to 13: contact with stream waters	Low-gray aragonite bushes and relatively darker spheroids to the top of thin section with a major structure at lamina 7/8 boundary made of thick dark organic matrix
33/Irma	lamina 1 to 26	Calcite rafts fabric (sparite) and mixed calcite and organic material (micrite) as laminoid-fenestral fabric

lamina to lamina. Carbonates exhibit different Mg and Sr content from one sample to another and from one lamina fabric to the other. For example, sparite calcite contains little Mg (≈ 0.05 wt%) and Sr (≈ 0.05 wt%). It contrasts with Mg-rich drusy calcite (Mg = 0.54 wt%, Sr = 0.05 wt%) and Sr-rich aragonite needles (Mg = 0.08 wt%; Sr = 0.58 wt%) (Table 3).

Carbon, Oxygen, and Strontium Isotope Compositions

Carbon (C) and oxygen (O) isotope compositions were determined on 13 laminae of sample 32 and 6 laminae from sample 33. The results are reported in Table 4 and Figure 8. Sample 32 displays variations in $\delta^{18}O$ values ranging between –1.22 and –6.13‰ VPDB and $\delta^{13}C$ values ranging between –10.75 and –6.52‰ VPDB. However, the central part of sample

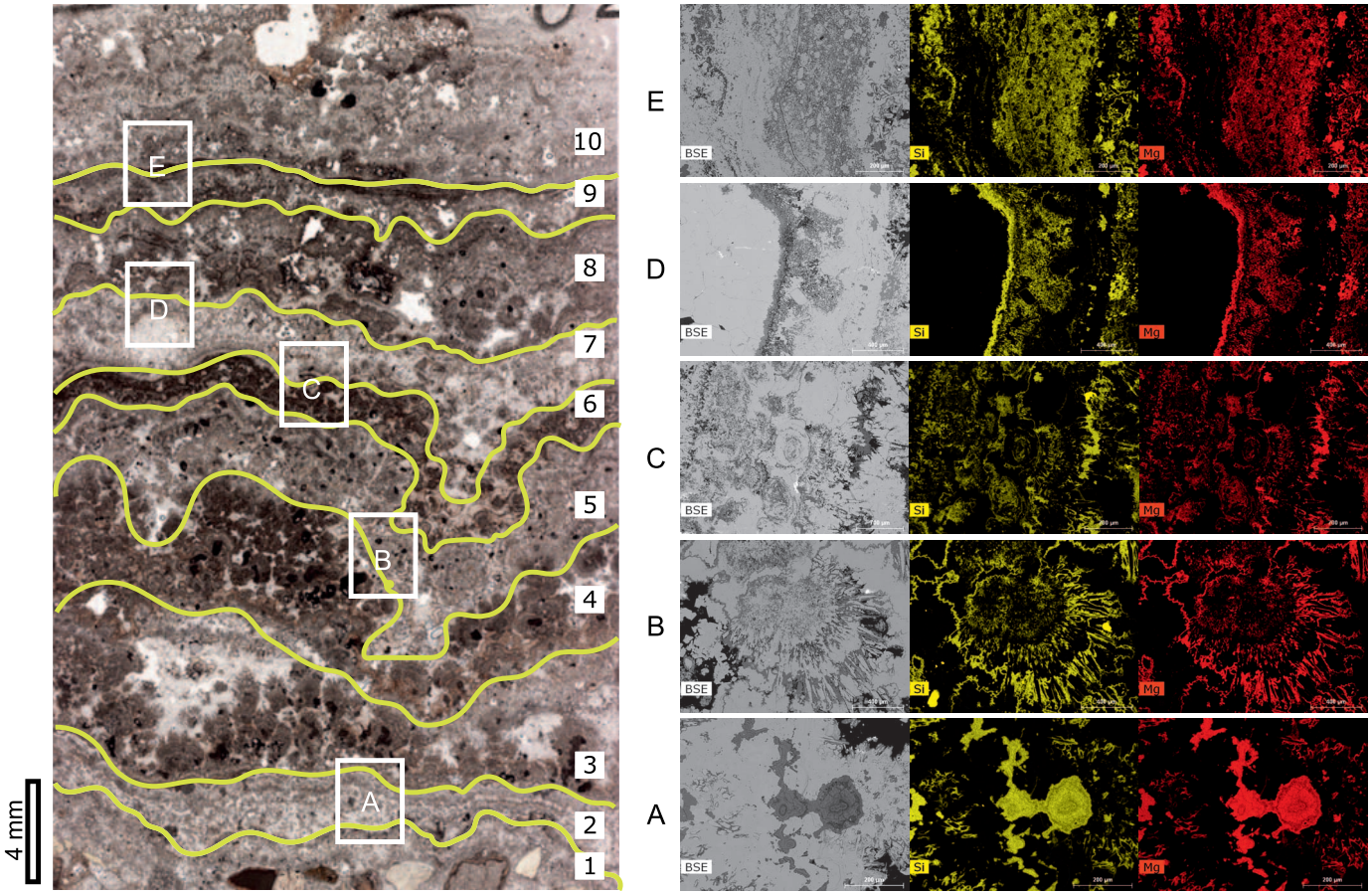

FIG. 5.—Detailed microscopic observations of sample 32 based on thin-section SEM chemical maps. **Zone A)** Pore spaces are filled with clays as shown by high concentration of Si, Mg, and Al elements at the transition between laminae 2 and 3. **Zone B)** Acicular calcium carbonate is approximately oriented toward the surface and grows from a micritic circular point. A thin film composed of Si, Al, Mg, and O overlies each generation of needle aragonite. **Zone C)** The transition between laminae 6 and 7 exhibits a variation from Si- and Mg-rich areas in the dark micritic lamina to Si, Mg, and Al-rich micro-oncoid, together with the occurrence of Si, Mg-rich µm-size grain (serpentine). **Zone D)** The sparry calcium carbonate in a pore in lamina 7 is haloed by Mg-Si-rich matrix. This lamina is irregularly thick. Some calcium carbonate crystals are contained in the matrix, the most remarkable example being the rectangular crystal in the dark matrix. A Ca carbonate layer formed over the matrix, first sparry calcite, then intergrown needle-like aragonite with the Si-Mg-rich matrix in contact with a pore. **Zone E)** The dark micritic lamina 9 appears to be composed of several rounded carbonates crystals in a Mg-Si-rich matrix.

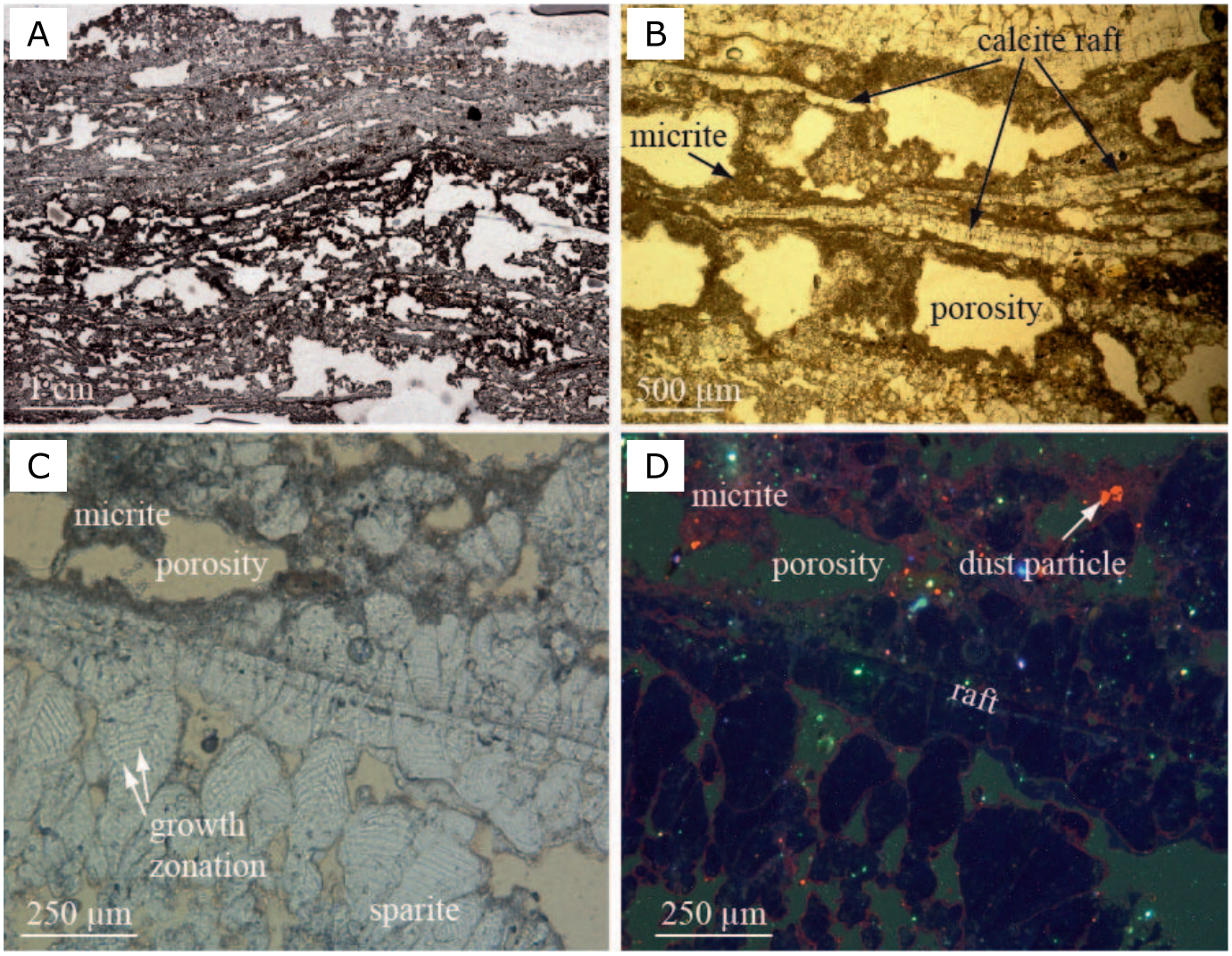

FIG. 6.—**A**, **B)** microscopy observations of sample 33 in transmitted polarized-light microscopy. **C**, **D)** Detail of a raft growth pattern in transmitted polarized-light microscopy and cathodoluminescence, respectively.

32 is characterized by a nearly constant $\delta^{18}O$ value with a mean value of –3.9‰ (VPDB). Some laminae of sample 33 show an extreme depletion in both ^{13}C and ^{18}O isotopes, with $\delta^{18}O$ values ranging from –16.54‰ to –10.12‰ (VPDB) and $\delta^{13}C$ values from –22.84‰ to –12.62‰ (VPDB).

While the $^{87}Sr/^{86}Sr$ ratio varies between 0.707282 and 0.707994 in sample 32, it is almost constant in sample 33 with a mean value of 0.70821, which is similar to that of hyperalkaline spring at this site (0.708164; Table 4). For sample 32, the most radiogenic Sr isotope ratio

TABLE 3.—*Electron microprobe analyses of calcium carbonates*.

Site	Lamina Petrofabric	Number of Analysis	Mg wt%	Sr wt%	Ca wt%	ln(Mg/Ca)	1 σD	ln(Sr/Ca)	1 σD
28	all	260	0.24	0.34	39.47	–6.0	1.8	–5.3	1.5
	dark lamina (isopach calcite)	120	0.44	0.05	39.49	–5.1	1.3	–6.8	1.3
	light lamina (aragonite fiber)	140	0.08	0.58	39.45	–7.2	1.8	–4.4	0.8
32	all	223	0.29	0.09	39.68	–5.5	1.4	–6.6	1.6
	lamina 2 (gothic arch calcite and aragonite bushes)	36	0.20	0.11	39.76	–5.5	1.1	–6.4	1.5
	lamina 6 (aragonite bush and calcite cement)	50	0.27	0.16	39.64	–5.7	1.6	–6.2	1.6
	lamina 7 (spheroid calcite)	30	0.39	0.03	39.60	–5.1	1.1	–7.1	1.0
	lamina 7 (in-filling sparite)	42	0.11	0.07	39.85	–6.6	1.4	–6.7	1.4
	lamina 8 (micro-spheroid calcite)	34	0.34	0.07	39.67	–5.1	1.5	–6.6	1.4
	lamina 10 (drusy calcite)	31	0.54	0.05	39.55	–4.6	1.0	–6.9	1.1
33	all (spar calcite)	29	0.05	0.05	39.90	–7.1	1.1	–6.7	0.9

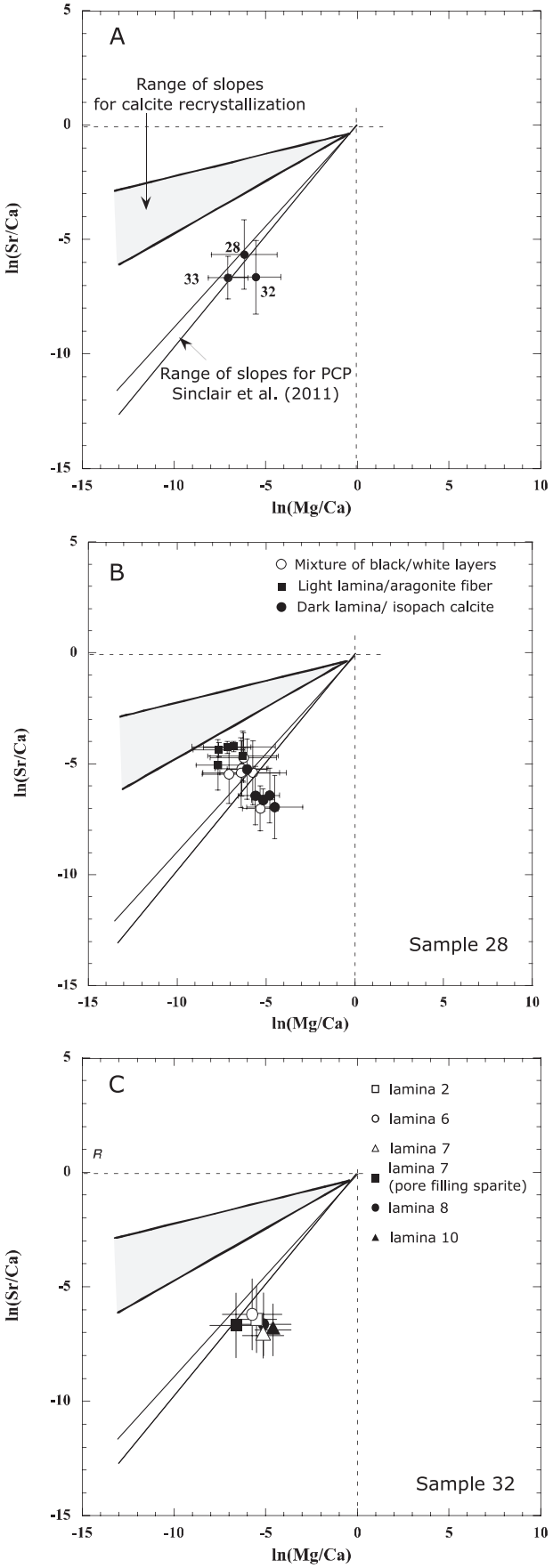

(close to surface-water signature) is measured in lamina 1 at the contact with the substrate, while the least radiogenic Sr isotope ratio (close to hyperalkaline spring signature) is measured in lamina 8, located next to a μm-thick Si- and Mg-rich layer (Table 4).

DISCUSSION

Linking Fabrics and Chemical Composition of Travertines

The distinctive fabrics of aragonite and calcite crystals seem to support the primary formation of these minerals (Renaut and Jones 1997). Nevertheless, it is necessary to decipher whether their morphologies express the environmental conditions at which they formed, or if they result from post-formation recrystallization. Divalent cations in aqueous solution (e.g., Mg, Sr, Ba, Mn, and Fe) may substitute for Ca in the crystal lattice during precipitation and recrystallization of carbonate, and when compared to their lamina fabric, can help elucidate primary versus secondary mineral phases. Our approach is based on previous karst waters and speleothem studies which showed that a constant slope in a ln(Sr/Ca) vs. ln(Mg/Ca) plot is due to a low Sr and Mg partition coefficient in calcite (Huang et al. 2001; Fairchild et al. 2000; Fairchild et al. 2006; McMillan et al. 2005; Johnson et al. 2006; Mattey et al. 2009), where dissolved Mg and Sr ions preferentially remain in solution while Ca precipitates as calcium carbonate. This chemical trend applied to speleothems has been named "prior calcite precipitation" (PCP). Based on a worldwide study of speleothems, Sinclair (2011) and Sinclair et al. (2012) were able to distinguish co-variation of Mg, Ca, and Sr concentrations that truly reflect environmental conditions compared to those induced by post-formation recrystallization. When applied to our samples as shown in Figure 7, the average ln(Mg/Ca) and ln(Sr/Ca) ratios of carbonate, without any distinction between carbonate fabrics, plot on or in error bars of the PCP slope (Fig. 7A), suggesting early calcite–water interaction, and not recrystallization.

However, the situation is more complicated when this approach is applied locally to the various carbonate fabrics of a travertine sample. For instance, in sample 28 (Fig. 7B), the dark sparitic lamina plots underneath the PCP slope whereas the white needle-like aragonite fabric plots above the PCP trend towards the range of calcite recrystallization. The combination of fabric and chemical compositions suggests at least partial carbonate recrystallization. Therefore, the geochemical record for climatic reconstruction is less useful for the cemented gravels in sample 28. Alternatively, all of the various carbonate fabrics of sample 32 plot slightly underneath the PCP trend (Fig. 7C), due potentially to different mixing proportions between hyperalkaline springs and runoff waters, which supply significant amounts of Mg and bicarbonate ions in solution compared to lack of supply of Mg from the hyperalkaline waters (Chavagnac et al. 2013b). Here, higher Mg content in carbonates suggests either an increase in runoff water proportion or a reduction of hyperalkaline spring-water influence. Finally, sparite calcite crystals of sample 33, which are formed at the air–water interface, show ln(Mg/Ca) and ln(Sr/Ca) ratios coherent with PCP processes, recording paleo-environmental conditions at the time of their precipitation.

Isotopic Records in Travertine

If well preserved, the carbon and oxygen isotopes can record environmental information in carbonate deposits (e.g., Darling et al. 2005; Lachniet 2009; Brady et al. 2010). The $\delta^{13}C$ values can be used to infer the origin of the carbon source, i.e., atmospheric CO_2 and/or DIC

←

FIG. 7.—Cross-plots of ln(Sr/Ca) vs. ln(Mg/Ca) according to Sinclair (2011) and Sinclair et al. (2012), **A)** the average bulk calcium carbonate composition of samples 28, 32, and 33, **B)** two fabrics average compositions of sample 28, and **C)** average chemical composition of the laminae defined for sample 32 (including the different fabrics identified).

TABLE 4.—*Thickness (cm), $\delta^{18}O_{(VPDB)}$, $\delta^{13}C_{(VPDB)}$ and $^{87}Sr/^{86}Sr$ ratios of individual laminae of samples 32 and 33. Calculated values of mixing contribution of hyperalkaline springs in % and paleotemperature are also reported (see text for details).*

Site-Lamina Number	Thickness	$\delta^{13}C_{PDB}$ ‰	$\delta^{18}0_{SMOW}$ ‰	$\delta^{18}O_{PDB}$ ‰	$^{87}Sr/^{86}Sr$ ($2\sigma_E$)	% Hyperalkaline Water in the Mixing Area	Calculated Paleotemperature in °C
Site 32-1	0.4	–7.71	29.48	–1.39	0.707994 (11)	33.3	14.8
Site 32-2	0.2	–8.08	29.66	–1.22	0.707947 (6)	35.9	14.1
Site 32-3	0.4	–6.52	26.66	–4.12	0.707813 (7)	43.5	27.5
Site 32-4	0.5	–6.91	26.84	–3.96	0.707761 (9)	46.5	26.6
Site 32-4 duplicata		–6.69	26.86	–3.93			26.5
Site 32-5	0.5	–7.26	27.1	–3.7	0.707784 (8)	45.2	25.4
Site 32-5 duplicata		–7.36	26.56	–4.23			28.0
Site 32-6	0.7	–7.89	26.99	–3.81	0.707749 (10)	47.2	25.9
Site 32-7	0.8	–7.86	27.23	–3.57	0.707695 (12)	50.3	24.8
Site 32-8	0.7	–10.75	27.31	–3.49	0.707282 (12)	74.5	24.4
Site 32-9	0.3	–10.52	27.14	–3.67	0.707390 (9)	68	25.2
Site 32-10	0.2	–9.77	26.66	–4.13	0.707513 (8)	60.9	27.5
Site 32-11	0.2	–9.24	27.13	–3.68	0.707743 (10)	47.5	25.3
Site 32-12	0.2	–9.53	26.60	–4.18	0.707419 (8)	66.3	27.8
Site 32-13	0.6	–8.94	24.60	–6.13	0.707438 (8)	65.3	37.9
Site 33-1	1	–12.62	20.48	–10.12	0.708163 (11)	n.d.	n.d.
Site 33-2	1	–15.53	19.69	–10.89	0.708214 (7)	n.d.	n.d.
Site 33-6	1.7	–21.27	16.03	–14.44	0.708197 (6)	n.d.	n.d.
Site 33-9	0.5	–20.26	15.64	–14.81	0.708260 (9)	n.d.	n.d.
Site 33-14	1.2	–22.84	14.05	–16.36	0.708209 (8)	n.d.	n.d.
Site 33-20	2	–21.96	13.86	–16.54	0.708177 (9)	n.d.	n.d.
spring 33bW1		n.m.	n.m.	n.m.	0.708164 (8)	n.d.	n.d.
spring 32W1		n.m.	n.m.	n.m.	0.706686 (8)	n.d.	n.d.
spring 33W1 (pH = 9.8)		n.m.	n.m.	n.m.	0.708614 (48)	n.d.	n.d.
spring 33W1 (pH = 10.5)		n.m.	n.m.	n.m.	0.708522 (18)	n.d.	n.d.
Calcite rafts[a]		–25.5	n.m.	–15.1	n.m.	n.d.	n.d.
		–25.6		–16.5		n.d.	n.d.
		–25.8		–16.8		n.d.	n.d.
		–24.8		–16.9		n.d.	n.d.
Rain water[b]		–7	–0.55 to –2.95	n.d.	n.m.	n.d.	n.d.
Ophiolite aquifer[c]		–13.6 to –15.6	–1.0 to –1.4	n.d.	n.m.	n.d.	n.d.
Surface water from wadi samail catchment[d]		–11.9 to –13.8	–1.60 to –2.41	n.d.	0.70844 to 0.70870	n.d.	n.d.

[a] Clark and Fontes (1992).
[b] Matter et al. (2005) and Weyhenmeyer (2000).
[c] Matter et al. (2005).
[d] Weyhenmeyer et al. (2002).
n.d. not determined.
n.m. not measured.

from runoff waters. The $\delta^{18}O$ is commonly used as a proxy for temperature and rainfall which is controlled by evaporation, condensation, climate, altitude, latitude, and distance from seawater (Dansgaard 1964).

Figure 8 presents the variation in $\delta^{18}O$ values as a function of $\delta^{13}C$ values for all laminae, and depicts two different trends. For sample 32, the $\delta^{18}O$ values are almost constant, while the $\delta^{13}C$ values are variable. A positive correlation is observed between atmospheric signature and calcite crust values for sample 33. These two distinctive trends can be interpreted through two different mechanisms: (1) hydration-hydroxylation reactions ($CO_{2(aq)} + H_2O \leftrightarrow HCO_3^-{}_{(aq)} + H^+$, and $CO_{2(aq)} + OH^- \leftrightarrow HCO_3^-{}_{(aq)}$, respectively) or (2) a kinetic effect during diffusion and dissolution of atmospheric CO_2 at the air–water interface (Neal and Stanger 1984; Clark and Fontes 1990; Clark et al. 1992).

For sample 32, the $\delta^{18}O$ values remain nearly constant for all laminae, apart from three, with variable $\delta^{13}C$ values (Fig. 8). The low occurrence of aragonite (less than 10%; Chavagnac et al. 2013a) does not seem to affect the oxygen isotope composition significantly, as the latter has a nearly constant value throughout the laminae. Constant $\delta^{18}O$ values likely indicate that hydration and hydroxylation reactions completely buffer the oxygen isotope composition of water (i.e., equilibrium state). Oxygen isotope equilibrium between $HCO_3^-{}_{(aq)}$ and H_2O is achieved, and therefore $\delta^{18}O$ values are not affected by kinetic effects (Mickler et al. 2006). Therefore, it is possible to calculate the equilibrium temperature using the following equation (Grossman 2012 and references therein):

$$T = 15.7 - 4.36 \times (\delta^{18}O_{cal} - \delta^{18}O_{water}) + 0.12 \times (\delta^{18}O_{cal} - \delta^{18}O_{water})^2 \quad (1)$$

Where T is temperature (°C), $\delta^{18}O_{cal}$ (carbonate) is given relative to the VPDB standard and $\delta^{18}O_{water}$ is the oxygen isotope composition of the water (in SMOW) (Table 4). A value of –1.6‰ (SMOW) was chosen for the $\delta^{18}O_{water}$, in line with water being a mixture between groundwater from the ophiolite aquifer at –1.0 to –1.4‰ (SMOW, Matter et al. 2005) and surface runoff waters at –1.6 to –2.41‰ (SMOW, Weyhenmeyer 2000). Sample 32 records wide temperature variations between 14.1 and 37.9°C (mean temperature of 25.4 ± 11°C). The lowest temperature of 14.1°C is striking. Nevertheless, it is not completely inconsistent with a drastic

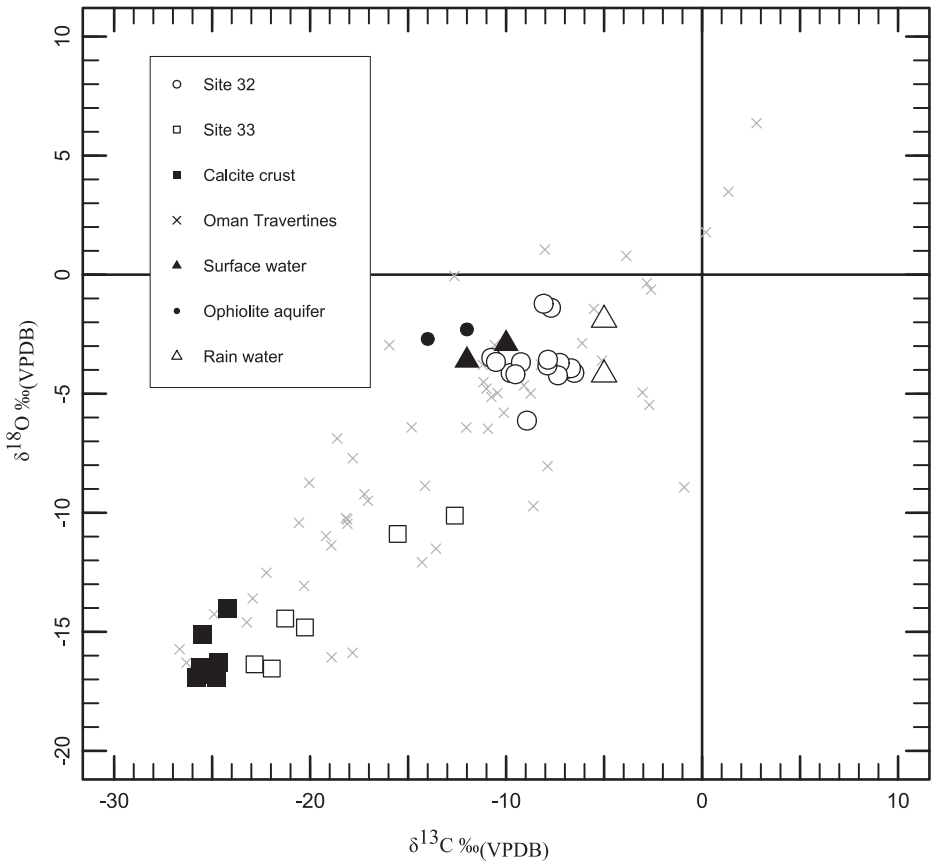

FIG. 8.—Plot of $\delta^{18}O$ values vs. $\delta^{13}C$ values of distinctive laminae of samples 32 and 33. Atmospheric CO_2 has a $\delta^{13}C$ value of –7‰. Calcite crust (black square): Clark et al. 1992; Oman travertines (cross): Clark and Fontes 1990, Mervine et al. 2014; Surface runoff waters (black triangle): Weyhenmeyer 2000; Ophiolite aquifer (black dot) and rain water (white triangle): Matter et al. 2005.

cooling of 6.5 ± 0.6°C for late Pleistocene Oman groundwaters (Weyhenmeyer et al. 2000). Unfortunately, the lack of sample ages severely restricts the interpretation of these paleo-temperatures in terms of a temporal climatic record.

In contrast, $\delta^{18}O$ and $\delta^{13}C$ values in sample 33 are close to calcite crust (sparite) values reported in Clark et al. (1992) (Fig. 8). Calcite precipitation is induced by evaporation and atmospheric conversion of gaseous CO_2 into carbonated species at the air–water interface. In this context, the coupled depletions in ^{18}O and ^{13}C result from both hydroxylation reactions and kinetic effects based on the difference in diffusion rates of $^{13}CO_2$ and $^{12}CO_2$ (Dietzel et al. 1992; Clark et al. 1990).

As a result, stable-isotope compositions alone are seriously limited to assess past climatic conditions without additional information on carbonate fabric and chemical composition. However, $\delta^{13}C$ values may be useful to elucidate the sources of carbon supply in this particular DIC-depleted environmental context of travertine formation.

Hyperalkaline Spring vs. Surface Runoff Waters and the Climatic Record

Further information about the climatic record may be provided by strontium isotope composition because each geological formation and solution exhibits distinctive $^{87}Sr/^{86}Sr$ ratios in this region. To confirm a potential contribution of surface runoff waters in travertine formation, the mixing equation of Albarède (1995) was used:

$$\left(^{87}Sr/^{86}Sr\right)_M = \left(\left(f_A{*}Sr_A{*}\left(^{87}Sr/^{86}Sr\right)_A\right) + \left((1-f_A){*}Sr_B{*}\left(^{87}Sr/^{86}Sr\right)_B\right)\right)/\left((f_A{*}Sr_A) + (1-f_A){*}Sr_B\right) \quad (2)$$

where A and B stand for two components, i.e., surface runoff and hyperalkaline waters, f_A the proportion of component A in the mixture, Sr_A and Sr_B are the Sr concentration of components A and B, respectively, and M is a mixture of these two components characterized by $(^{87}Sr/^{86}Sr)_M$ isotope composition. In our study, the measured $^{87}Sr/^{86}Sr$ from each laminae of travertine represents the mixture M. For the calculations, Sr concentrations of 5.7 μmol l^{-1} and 6.1 μmol l^{-1} and $^{87}Sr/^{86}Sr$ ratios of 0.70860 and 0.706686 were taken for surface runoff waters (Weyhenmeyer 2000) and hyperalkaline waters, respectively (Chavagnac et al. 2013b). Sr concentration and isotope composition of hyperalkaline waters are considered constant, as the springs are perennial. The results are presented in Table 4.

Figure 9A illustrates the variation in $^{87}Sr/^{86}Sr$ ratios, $\delta^{18}O$ and $\delta^{13}C$ values as a function of laminae thickness throughout sample 32. Strikingly, the Sr isotope signature co-varies with the $\delta^{13}C$ values throughout sample 32, whereby the contribution of surface runoff waters varied from 25 to 67%. While the contribution of each end member is almost constant (about 45–50%) in laminae 3 to 7, a 25% decrease is noted at the transition between laminae 7 and 8, where the $^{87}Sr/^{86}Sr$ ratios decrease from 0.707695 to 0.707282 (Fig. 9). This observation seems to indicate a significant change in the hydrological regime where the contribution from surface water becomes subsidiary to the spring water. This is also sustained by the strong accumulation of Si- and Mg-rich organic material observed in microscopic scale at this transition, suggesting less surface runoff water. In comparison, the co-variation in Sr and C isotope compositions from laminae 8 to 11 indicates an increasing contribution of surface runoff water from 25 to 34% (Fig. 9).

Additionally, the variation in $\delta^{18}O$ values of sample 32 are similar to what was obtained for a speleothem in Hoti cave (from –1.39‰ to –6.13‰ for sample 32, from –2 to –6‰ for the Hoti Cave's speleothem; Burns et al. 2001; Fleitmann et al. 2007). For the speleothem with a constant

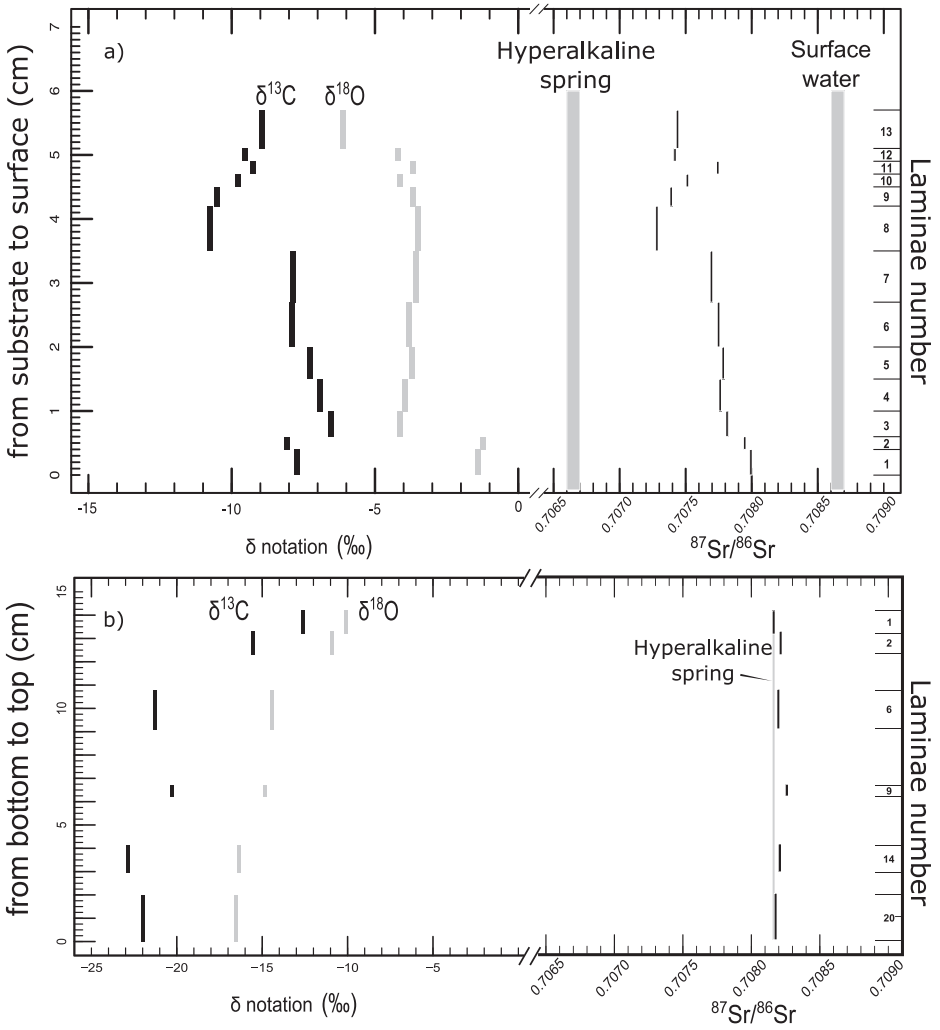

FIG. 9.—Variations of $\delta^{18}O$ and $\delta^{13}C$ values and $^{87}Sr/^{86}Sr$ ratio along the **A)** sample 32 and **B)** sample 33. Sr-isotope composition of surface runoff water are from Weyhenmeyer 2000.

temperature in the cave, the reason for such variations of the $\delta^{18}O$ values are interpreted as being due to the northward shift of the ITCZ (Burns et al. 2001; Fleitmann et al. 2007). However, in our study we do not have any temporal constraint of travertine formation; it is therefore difficult to infer with confidence the $\delta^{18}O$ signature of the dominating rain waters. So because neither temperature nor sources are well constrained, in terms of the past climatic record, we can conclude only that the contribution of surface waters in the mixing area has fluctuated through time.

For comparison, all laminae of sample 33 exhibit $^{87}Sr/^{86}Sr$ ratios very close to the signature of hyperalkaline spring water (i.e., 0.708164), indicating no evidence of mixing with surface waters (Fig. 9B). In contrast, large variations in $\delta^{13}C$ values are observed (between –12.6 and –22.8‰ VPDB, Fig. 9B). In this sample, the kinetic effect induced by the diffusion of $CO_{2(g)}$ at the air–water interface is the major process modifying the C isotope compositions. The unique source of C in sample 33 is atmospheric $CO_{2(g)}$, i.e., a potentially arid climate, as there is no evidence of surface runoff waters based on both $^{87}Sr/^{86}Sr$ ratios and the link between carbonate fabric and chemical composition.

In summary, the stable-isotope and radiogenic-isotope signatures of laminae document the paleo-activity of hyperalkaline spring waters through time, and contribute to a better understanding of the mechanisms leading to the formation of travertine in a DIC-depleted environment. $^{87}Sr/^{86}Sr$ ratios have shown to be a useful tracer for quantifying surface runoff water contribution in this setting.

DIC-Depleted vs. DIC-Enriched Environment for Continental Carbonate Formation

In Oman, the close relationship between the occurrence of travertine and the DIC-depleted hyperalkaline spring waters contrasts radically with most of continental travertines that precipitate from DIC-enriched waters (Capezzuoli et al. 2014). A fundamental question arises from this particular mode of formation: What do the stable-isotope compositions of carbonates record when they are formed in such contrasted DIC environments?

Figure 10 compares the variations in $\delta^{13}C$ and $\delta^{18}O$ values obtained in this study with data presented in the literature and obtained on both DIC-depleted and DIC-enriched environments. Each carbonate deposit defines different fields, although some data from Oman travertines overlap with tufa. All carbonates formed under continental DIC-depleted hyperalkaline conditions define a linear and positive trend between the negative values of $\delta^{13}C$ and $\delta^{18}O$ values. This is in line with the data acquired on carbonate deposits found at the Liguria hyperalkaline waters (Teboul et al. 2016). In addition, carbonates associated with submarine hyperalkaline springs (e.g., the Lost City hydrothermal field located at 30° N along the Mid-Atlantic Ridge, 800 m water depth; Kelley et al. 2001), exhibit positive $\delta^{13}C$ and $\delta^{18}O$ values, at the top end of the linear trend defined by carbonates found at continental DIC-depleted hyperalkaline conditions. Their stable-isotope signature is consistent with marine carbonates, for which the main source of carbon is provided by seawater bicarbonate ions. In general terms, the

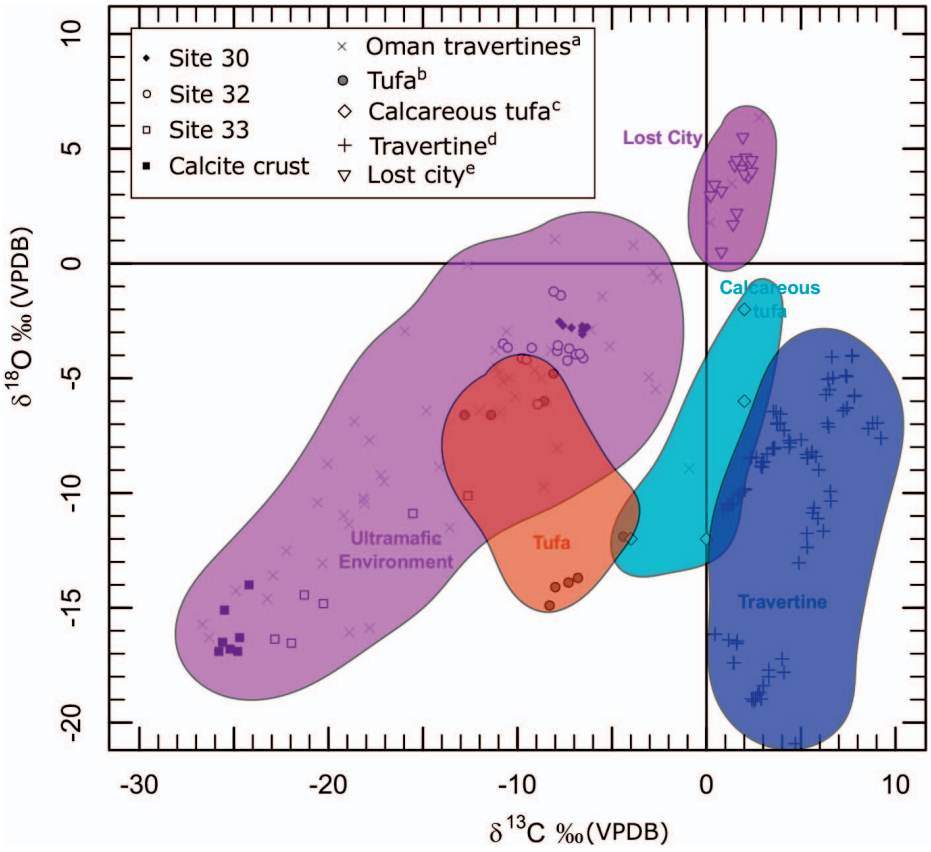

FIG. 10.—Plot of $\delta^{18}O$ values vs. $\delta^{13}C$ values of distinctive laminae (travertine 32 and 33). [a] Mervine et al. 2014; [b] Caton 2009, Janssen et al. 1999; [c] Cremaschi et al. 2010, Pola et al. 2014, Chafetz and Lawrence 1994, Guo et al. 1996, Kele et al. 2008, Fouke et al. 2001; [d] O'Neil and Barnes 1971, Schwarzenbach et al. 2013, Teboul et al. 2016; [e] Früh-Green et al. 2003, Dubinina et al. 2007.

variation of stable-isotope signatures reflects the source of carbon supply and the processes that led to carbonate formation, i.e., hydration and hydroxylation reactions and/or diffusion of $CO_{2(g)}$ at the air–water interface, rather than climatic records.

For DIC-enriched environment, Gandin and Capezzuoli (2008) demonstrated that calcareous tufa exhibits negative $\delta^{13}C$ and $\delta^{18}O$ values that represent outgassing of meteoric and soil derivation (Pentecost 2005) and cool temperature and saturation levels of spring water (Chafetz and Lawrence 1994), respectively. Photosynthetic effects associated with development of microorganisms remained very limited. The C and O stable-isotope compositions reflect the signature of the water from which the calcareous tufa derived, i.e., the local climatic regime. Tufas present negative but intermediate stable-isotope compositions between "DIC-depleted" travertine and calcareous tufa. This reflects the physicochemical signature of karstic water and microorganism activity (Capezzuoli et al. 2014). Finally, "DIC-enriched" travertines are characterized by positive $\delta^{13}C$ but negative $\delta^{18}O$ values, which illustrate the complex interplay between the source of groundwater thermally heated and tectonic and volcanic activity. In the latter case, little information can be obtained for the past climatic record, but it provides an innovative way to monitor past volcanic carbon dioxide emissions (Capezzuoli et al. 2014).

To summarize, carbonate deposits have a great potential for better defining the physicochemical environmental conditions and the processes that led to their formation. In their study of calcitic–aragonitic travertine–tufa deposits (DIC-enriched environment), Teboul et al. (2016) argue that combining geochemical tracers (Ba and Sr among others) with stable-isotope compositions provide valuable constraints on hydrogeological and paleo-hydrogeological circulation. Based on the present study (DIC-depleted environment), the combination of geochemical tracers with fabric description provides a crucial indicator of crystallization versus recrystallization at the time of carbonate formation, and thus a potential proxy of past environmental conditions. When these observations are combined with isotopic tracers such as O, C, and Sr, then the environmental conditions can be better defined in terms of surface-runoff contribution and source of carbon supply.

Sequestration of Atmospheric CO_2 during Travertine Formation

Precipitation rate of travertine from hyperalkaline springs is variable, and will depend on the amount of calcium available, spring flow rate, and temperature, among other parameters (Pentecost 2005). The amount of atmospheric $CO_{2(g)}$ uptake and calcium carbonate amount sequestered in travertine can be estimated either based on the volume and age of the travertine terraces (e.g., Mervine et al. 2014), or from the chemistry and flow rate of spring waters. In the latter case, the assumption is made that calcite precipitation occurs until thermodynamic equilibrium with atmospheric P_{CO2} is reached, or evaporation is total. Calcite was taken as the reference for calculations as it is the main mineral found in travertine (it is also the more stable mineral versus aragonite over geologic time). Volume of calcite precipitate was estimated for sites 28, 32, and 33 based on average chemistry analyses (data from this study and Pentecost 2005) and flow rate at spring (unpublished data), according to the following equation:

$$V_{travertine} = \frac{V_{cal}}{1-\phi} = \frac{Q \times v_{cal}}{1-\phi} \int_t \Delta Ca\, dt \qquad (3)$$

$V_{travertine}$ is the volume of precipitated travertine (which can also be expressed as a rate, i.e., $m^3\ yr^{-1}$, when divided by time t), V_{cal} is the volume of precipitated calcite, ϕ is the porosity of travertine, υ_{cal} is the molar volume of calcite ($m^3\ mol^{-1}$), and ΔCa is the difference in calcium concentration between the spring ($[Ca_i]$) and the calcium-depleted solution

TABLE 5.—*Results of geochemical modeling with CHESS giving an estimate of CO_2 uptake and travertine deposits rate (per year). Input data: $[CO_2] = 280$ ppm, porosity = 0.35, data of $[Ca_i]$ from Chavagnac et al. (2013b) and Q from (Chavagnac, unpublished data).*

	Site 28	Site 32	Site 33	Average for 50 sites
Q (l s^{-1})	0.5	0.2	0.1	25
$[Ca_i]$ spring (M)	1.18 10^{-3}	1.88 10^{-3}	1.09 10^{-4}	1.67 10^{-3}
pH_i (modelling result)	11.0	11.5	11.6	
SI calcite (log)	1.34	1.73	0.40	
SI aragonite (log)	1.19	1.58	0.25	
SI Monohydrotalcite (log)	0.46	0.87	–0.14	
$[Ca_{eq}]$ (M)	2.18 10^{-4}	1.24 10^{-4}	4.53 10^{-5}	1.29 10^{-4}
Hypothesis 1: thermodynamic equilibrium is reached				
CO_2 sequestered (kg yr^{-1})	666	487	9	5.4 10^4
Vtravertine /t (m^3 yr^{-1})	8.6	6.3	0.1	692
Hypothesis 2: evaporation is total				
CO_2 sequestered (kg yr^{-1})	817	522	15	5.8 10^4
Vtravertine /t (m^3 yr^{-1})	10.5	6.7	0.2	749

(equal to $[Ca_{eq}]$ when thermodynamic equilibrium is reached, or to $[Ca_{ev}] = 0$ M when evaporation is total). $[Ca_{eq}]$ was calculated from geochemical modeling using CHESS (Van der Lee 1998). First, the chemical equilibrium of the solutions at the spring was calculated using the CHESS database and the Debye-Hückel model of activity correction. Charge balance was set on OH^- and DIC was imposed through a low fugacity of CO_2 (resulting in values from 10^{-12} to 3×10^{-10} atm). Due to the low amount of DIC, all the discharge waters are undersaturated with respect to calcite. The calculated pH (pH_i) is in good agreement with values measured in the field (Table 5). Secondly, a fugacity of CO_2 of 2.8×10^{-4} atm was imposed to mimic equilibrium with Quaternary interglacial atmospheric P_{CO2}. Dissolution of CO_2 from the atmosphere into the waters causes oversaturation with respect to calcite, aragonite, and mono-hydrotalcite (except for site 33, where water remains undersaturated with mono-hydrotalcite). The saturation index (SI) of calcite is higher than 1, enabling precipitation, but it is worth noting that SI for site 33 is smaller than the critical supersaturation of 4–10 reported in Pentecost (2005); there, precipitation must be triggered by evaporation, which is in agreement with the observation of calcite rafts. Given an average porosity of 35% (Noiriel, unpublished data), the volume of travertine deposit varies for site between $\approx$ 0.1 and $\approx$ 10 m^3 yr^{-1}. Calculation assuming about 50 travertine deposits in Oman for a cumulative flow rate of 25 l s^{-1} (i.e., Q = 0.5 l s^{-1} in average), an average $[Ca_i] = 1.67$ mM, and an estimate of the total travertine area in the Samail Ophiolite of 10^7 m^2 (Kelemen and Matter 2008; Mervine et al. 2014) gives a deposition rate of $\approx$ 0.05 mm yr^{-1} sequestering $\approx$ 5 10^4 kg CO_2 yr^{-1}. This value is three orders of magnitude smaller than the one estimated by Mervine et al. (2014) on the same number of travertine deposits. As $[Ca_i]$ is generally between 1 and 2 mM for hyperalkaline springs (Chavagnac et al. 2013b), the flow rate represents the largest uncertainty in the calculation, which could have been higher in the past, leading to a higher deposition rate (regardless, it is not likely to be three orders of magnitude higher than actual). CO_2 can also be transformed into organic matter through biological processes (e.g., photosynthesis), although its content in travertine does not generally exceed a few percent (Pentecost 2005). On the other hand, a lower P_{CO2} (e.g., during Quaternary glacial periods) or a saturation index higher than 0 (i.e., equilibrium not reached and Ca being exported through streams after mixing with runoff waters) will counterbalance the deposition rate.

From equilibrium calculations, it appears that the best conditions to store CO_2 as calcium carbonate depend on initial Ca concentration and surface waters mixing with hyperalkaline springs. It seems clear that the rate of sequestration of atmospheric CO_2 also depends on the mechanism of precipitation, which should be accounted for large-scale evaluation.

CONCLUSION

A detailed multi-disciplinary approach, from macroscopic to microscopic scale, has been accomplished on three travertine samples formed under DIC-depleted hyperalkaline environments in order to 1) assess the relationship between the petrologic features and fabrics and the geochemical and isotopic signatures, and 2) discuss the potential of these deposits as proxies for past climatic record and sequestration of atmospheric CO_2. The samples illustrate two distinct mechanisms of calcium carbonate formation, either from mixing of hyperalkaline and surface runoff waters (sample 28 and 32) or from dissolution of atmospheric $CO_{2(g)}$ into hyperalkaline waters (sample 33).

We conclude:

- Travertines as a whole are characterized by chemical compositions, expressed in terms of Mg, Ca, and Sr contents, consistent with "prior calcite precipitation" (PCP) process, i.e., the record of environmental conditions at the time of their formation. However, by comparing trace-element concentrations from one fabric to the other (sparite, drusy, spheroid calcite to aragonite micro-stalactic and needle-like aragonite), it is possible to distinguish between recrystallization conditions (sample 28) and temporal variation of environmental conditions (samples 32 and 33).
- The linear and positive variations in $\delta^{18}O$ and $\delta^{13}C$ values between laminae reflects two different mechanisms: (1) hydration-hydroxylation reactions from which a paleo-temperature of water can be extracted (sample 32) and/or (2) kinetic effects induced by diffusion of CO_2 at the air–water interface (sample 33).
- The combined variations in O, C, and Sr isotope signatures between laminae document the paleo-activity of hyperalkaline spring and surface runoff waters through formation time scales. The $^{87}Sr/^{86}Sr$ ratio represents a useful tracer for quantifying surface runoff water contribution, and acts as an indicator of rainfall intensity.
- In the framework of continental carbonates, travertine formed in a DIC-depleted environment exhibit $\delta^{18}O$ and $\delta^{13}C$ values that contrast to those formed in a DIC-enriched environment. With the prospect of assessing the past climatic record, it appears necessary 1) to combine the detailed petrological observations with chemical compositions at the lamina to unravel crystallization versus recrystallization processes, and 2) to corroborate radiogenic and stable-isotope analyses for quantifying precipitation intensity.
- Finally, the influence of climate should be addressed when quantifying carbonation rates, as shown by the range of CO_2 sequestered in the different scenarios illustrated by our samples (from 9 kg CO_2 yr^{-1} to 522 kg CO_2 yr^{-1}).

SUPPLEMENTAL MATERIAL

An Appendix is available from JSR's Data Archive: http://sepm.org/pages.aspx?pageid=229.

ACKNOWLEDGMENTS

We acknowledge the technical help of Chantal Perrache (LMV Saint-Etienne) and Michel Thibault, Jonathan Prunier, and Pierre Brunet (GET, Toulouse) for the analyses of O and C isotopes, mineralogical, geochemical, and Sr isotopes, respectively. We also acknowledge the comments of two anonymous reviewers and the editors, which greatly improved the quality and presentation of the data reported in this study.

REFERENCES

Abily, B., and Ceuleneer, G., 2013, The dunitic mantle–crust transition in the Oman ophiolite: residue of melt–rock interaction, cumulates from high-MgO melts, or both?: Geology, v. 41, p. 67–70.

Abrajano, T.A., Sturchio, N.C., Bohlke, J.K., Lyon, G.L., Poreda, R.J., and Stevens, C.M., 1988, Methane-hydrogen gas seeps, Zambales Ophiolite, Philippines: deep or shallow origin?: Chemical Geology, v. 71, p. 211–222.

Alabaster, T., Pearce, J., and Malpas, J., 1982, The volcanic stratigraphy and petrogenesis of the Oman ophiolite complex: Contributions to Mineralogy and Petrology, v. 81, p. 168–183.

Albarède, F., 1995, Introduction to Geochemical modelling: Cambridge University Press, Cambridge, UK, 543 p.

Amri, I., Benoit, M., and Ceuleneer, G., 1996, Tectonic setting for the genesis of oceanic plagiogranites: evidence from a paleo-spreading structure in the Oman ophiolite: Earth and Planetary Science Letters, v. 139, p. 177–194.

Arenas, C., Vasquez-Urbez, M., Auqué, L., Sancho, C., Osacar, C., and Pardo, G., 2014, Intrinsic and extrinsic controls of spatial and temporal variations in modern fluvial tufa sedimentation: a thirteen-year record from a semi-arid environment: Sedimentology, v. 61, p. 90–132.

Barnes, I., and O'Neil, J.R., 1969, Relationship between fluids in some fresh alpine-type ultramafics and possible modern serpentinization, western United States: Geological Society of America, Bulletin, v. 80, p. 1947–1960.

Barnes, I., Lamarche, V., Jr., and Himmelberg, G., 1967, Geochemical evidence of present-day serpentinization: Science, v. 156, p. 830–832.

Barnes, I., O'Neil, J.R., and Trescases, J.-J., 1978, Present day serpentinization in New Caledonia, Oman and Yugoslavia: Geochimica et Cosmochimica Acta, v. 42, p. 144–145.

Boudier, F., and Coleman, R.G., 1981, Cross-section through the peridotite in the Samail ophiolite, Southeastern Oman mountains: Journal of Geophysical Research, v. 86, p. 2573–2592.

Boulart, C., Chavagnac, V., Monnin, C., Delacour, A., Ceuleneer, G., and Hoareau, G., 2013, Differences in gas venting from ultramafic-hosted warm springs: the example of Oman and voltri ophiolites: Ofioliti, v. 38, p. 143–156.

Brady, A.L., Slater, G.F., Omelon, C.R., Southam, G., Druschel, G., Andersen, D.T., Hawes, I., Laval, B., and Lim, D.S.S., 2010, Photosynthetic isotope biosignatures in laminated micro-stromatolitic and non-laminated nodules associated with modern, freshwater microbialites in Pavilion Lake, B.C.: Chemical Geology, v. 274, p. 56–67.

Bruni, J., Canepa, M., Chiodini, G., Cioni, R., Cipolli, F., Longinelli, A., Marini, L., Ottonello, G., and Vetuschi Zuccolini, M., 2002, Irreversible water–rock mass transfer accompanying the generation of the neutral, Mg–HCO_3 and high-pH, Ca–OH spring waters of the Genova province, Italy: Applied Geochemistry, v. 17, p. 455–474.

Burns, S.J., Fleitmann, D., Matter, A., Neff, U., and Mangini, A., 2001, Speleothem evidence from Oman for continental pluvial events during interglacial periods: Geology, v. 29, p. 623–626.

Capezzuoli, E., Gandin, A., and Pedley, M., 2014, Decoding tufa and travertine (fresh water carbonates) in the sedimentary record: The state of the art: Sedimentology, v. 61, p. 1–21.

Caton, J.C., 2009, Environmental controls on the formation and isotopic composition of a laminated tufa in Red Butte canyon, Utah: University of Utah, 119 p.

Ceuleneer, G., Monnereau, M., and Amri, I., 1996, Thermal structure of a fossil mantle diaper inferred from the distribution of mafic cumulates: Nature, v. 379, p. 149–153.

Chafetz, H., and Lawrence, J., 1994, Stable isotopic variability within modern travertines: Géographie Physique et Quaternaire, v. 48, p. 257–273.

Chavagnac, V., Ceuleneer, G., Monnin, C., Lansac, B., Hoareau, G., and Boulart, C., 2013a, Mineralogical assemblages forming at hyperalkaline warm springs hosted on ultramafic rocks: a case study of Oman and Ligurian ophiolites: Geochemistry Geophysics Geosystems, v. 14, p. 2474–2495.

Chavagnac, V., Monnin, C., Ceuleneer, G., Boulart, C., and Hoareau, G., 2013b, Characterization of hyperalkaline fluids produced by low-temperature serpentinization of mantle peridotites in the Oman and Ligurian ophiolites: Geochemistry Geophysics Geosystems, v. 14, p. 2496–2522.

Cipolli, F., Gambardella, B., Marini, L., Ottonello, G., and Zuccolini, M., 2004, Geochemistry of high-pH waters from serpentinites of the Gruppo di Voltri (Genova, Italy) and reaction path modelling of CO_2 sequestration in serpentinite aquifers: Applied Geochemistry, v. 19, p. 787–802.

Clark, I.D., and Fontes, J.-C., 1990, Paleoclimatic reconstruction in Northern Oman based on carbonates from hyperalkaline groundwaters: Quaternary Research, v. 33, p. 320–336.

Clark, I.D., Fontes, J.-C., and Fritz, P., 1992, Stable isotope disequilibria in travertine from high pH waters: laboratory investigations and field observations from Oman: Geochimica et Cosmochimica Acta, v. 56, p. 2041–2050.

Coleman, R., 1981, Tectonic setting for ophiolite obduction in Oman: Journal of Geophysical Research, v. 86, p. 2497–2508.

Cremaschi, M., Zerboni, A., Spötl, C., and Felletti, F., 2010, The calcareous tufa in the Tadart Acacus Mt. (SW Fezzan, Libya), an early Holocene palaeoclimate archive in the central Sahara: Palaeogeography, Palaeoclimatology, Palaeoecology, v. 287, p. 81–94.

Dansgaard, W., 1964, Stable isotopes in precipitation: Tellus, v. 16, p. 436–468.

Darling, W.G., Bath, A.H., Gibson, J.J., and Rozanski, K., 2006, Chapter 1, Isotopes in Water, *in* Leng, M.J., ed., Isotopes in Paleoenvironmental Research: Dordrecht, 66 p.

Dietzel, M., Usdowski, E., and Hoefs, J., 1992, Chemical and $^{13}C/^{12}C$- and $^{18}O/^{16}O$-isotope evolution of alkaline drainage waters and the precipitation of calcite: Applied Geochemistry, v. 7, p. 177–184.

Dubinina, E., Chernyshew, I., Bortnikov, N., Lein, A., Sagalevich, A., Gol'tsman, Y., Bairova, E., and Mokhov, A., 2007, Isotopic–geochemical characteristics of the lost city hydrothermal field: Geochemistry International, v. 45, p. 1131–1143.

Fairchild, I., Borsato, A., Tooth, A.F., Frisia, S., Hawkesworth, C., Huang, Y., McDermott, F., and Spiro, B., 2000, Controls on trace element (Sr-Mg) compositions of carbonate cave waters: implications for speleothem climatic records: Chemical Geology, v. 166, p. 255–269.

Fairchild, I.J., Smith, C.L., Baker, A., Fuller, L., Spötl, C., Mattey, D., McDermott, F., and Edinburgh Ion Microprobe Facility (E.I.M.F.), 2006, Modification and preservation of environmental signals in speleothems: Earth-Science Reviews, v. 75, p. 105–153.

Fleitmann, D., Burns, S.J., Neff, U., Mangini, A., and Matter, A., 2003, Changing moisture sources over the last 330,000 years in Northern Oman from fluid-inclusion evidence in speleothems: Quaternary Research, v. 60, p. 223–232.

Fleitmann, D., Burns, S.J., Neff, U., Mudelsee, M., Mangini, A., and Matter, A., 2004, Palaeoclimatic interpretation of high-resolution oxygen isotope profiles derived from annually laminated speleothems from Southern Oman: Quaternary Science Reviews, v. 23, p. 935–945.

Fleitmann, D., Burns, S.J., Mangini, A., Mudelsee, M., Kramers, J., Villa, I., Neff, U., Al-Subbary, A.A., Buettner, A., Hippler, D., and Matter, A., 2007, Holocene ITCZ and Indian monsoon dynamics recorded in stalagmites from Oman and Yemen (Socotra): Quaternary Science Reviews, v. 26, p. 170–188.

Flügel, E., 2004, Microfacies of Carbonate Rocks: Analysis, Interpretation and Application: Berlin, Springer-Verlag, 996 p.

Ford, T.D., and Pedley, H.M., 1996, A review of tufa and travertine deposits of the world: Earth-Science Reviews, v. 41, p. 117–175.

Fouke, B., 2011, Hot-spring systems geobiology: abiotic and biotic influences on travertine formation at Mammoth Hot Springs, Yellowstone National Park, USA: Sedimentology, v. 58, p. 170–219.

Fouke, B., Farmer, J., Des Marais, D., Pratt, L., Sturchio, N., Burns, P., and Discipulo, M., 2001, Depositional facies and aqueous–solid geochemistry of travertine-depositing hot springs (Angel Terrace, Mammoth Hot Springs, Yellowstone National Park, USA): Journal of Sedimentary Research, v. 70, p. 565–585.

Fruh-Green, G.L., Kelley, D.S., Bernasconi, S.M., Karson, J.A., Ludwig, K.A., Butterfield, D.A., Boschi, C., and Proskurowski, G., 2003, 30,000 years of hydrothermal activity at the Lost City vent field: Science, v. 301, p. 495–498.

Fuchs, M., and Buerkert, A., 2008, A 20 ky sediment record from the Hajar Mountain range in N-Oman, and its implication for detecting arid–humid periods on the southeastern Arabian Peninsula: Earth and Planetary Science Letters, v. 265, p. 546–558.

Gandin, A., and Capezzuoli, E., 2008, Travertine versus calcareous tufa: distinctive petrologic features and related stable isotopes signature: Il Quaternario, v. 21, p. 125–136.

Gandin, A., and Capezzuoli, E., 2014, Travertine: distinctive depositional fabrics of carbonates from thermal spring systems: Sedimentology, v. 61, p. 264–290.

Grossman, E., 2012, Applying oxygen isotope paleothermometry in deep time, *in* Ivany L.C., and Huber, B.T., eds., Reconstructing Earth's Deep-Time Climate: The State of the Art in 2012: Paleontological Society Short Course, The Paleontological Society Papers, v. 18, p. 39–67.

Guo, L., Andrews, J., Riding, R., Dennis, P., and Dresser, Q., 1996, Possible microbial effects on stable carbon isotopes in hot travertine: Journal of Sedimentary Research, v. 66, p. 468–473.

Huang, H., Fairchild, I., Borsato, A., Frisia, S., Cassidy, N., McDermott, F., and Hawkesworth, C., 2001, Seasonal variations in Sr, Mg and P in modern speleothems (Grotta di Ernesto, Italy): Chemical Geology, v. 175, p. 429–448.

Janssen, A., Swennen, R., Podoor, N., and Keppend, E., 1999, Biological and diagenetic influence in Recent and fossil tufa deposits from Belgium: Sedimentary Geology, v. 126, p. 75–95.

Johnson, K., Hu, C., Belshaw, N., and Henderson, G., 2006, Seasonal trace-element and stable-isotope variations in a Chinese speleothem: the potential for high-resolution paleomonsoon reconstruction: Earth and Planetary Science Letters, v. 244, p. 394–407.

Juteau, T., Ernewein, M., Reuber, I., Whitechurch, H., and Dahl, R., 1988, Duality of magmatism in the plutonic sequence of the Semail Nappe, Oman: Tectonophysics, v. 151, p. 107–126.

Kele, S., Demémy, A., Siklosy, Z., Németh, T., Toth, M., and Kovacs, M., 2008, Chemical and stable isotope composition of recent hotwater travertines and associated thermal waters, from Egerszalòk, Hungary: depositional facies and non-equilibrium fractionation: Sedimentary Geology, v. 211, p. 53–72.

Kelemen, P.B., and Matter, J., 2008, *In situ* carbonation of peridotite for CO_2 storage: National Academy of Sciences [U.S.A.], Proceedings, v. 105, p. 17295–17300.

Kelemen, P.B., Matter, J., Streit, E.E., Rudge, J.F., Curry, W.B., and Blusztajn, J., 2011, Rates and mechanisms of mineral carbonation in peridotite: natural processes and recipes for enhanced, *in situ* CO_2 capture and storage: Annual Review of Earth and Planetary Sciences, v. 39, p. 545–576.

Kelley, S.D., Karson, J.A., Blackman, D.K., Fruh-Green, G.L., Butterfield, D.A., Lilley, D.M., Olson, E.J., Schrenk, M.O., Roell, K.K., Lebon, G.T., Rivizzigno, P., and the AT3-60 Shipboard Party, 2001, An off-axis hydrothermal vent field near the Mid-Atlantic Ridge at 30° N: Nature, v. 412, p. 145–149.

Kwarteng, A.Y., Dorvlo, A.S., and Kumar, G.T.V., 2009, Analysis of a 27-year rainfall data (1977–2003) in the Sultanate of Oman: International Journal of Climatology, v. 29, p. 605–617.

Lachniet, M.S., 2009, Climatic and environmental controls on speleothem oxygen-isotope values: Quaternary Science Reviews, v. 28, p. 412–432.

Launay, J., and Fontes, J.C., 1985, Les sources thermales de Prony (Nouvelle Calédonie) et leurs précipités chimiques exemple de formation de brucite primaire: Géologie de France, v. 1, p. 83–100.

Matter, J.M., Waber, H.N., Loew, S., and Matter, A., 2005, Recharge areas and geochemical evolution of groundwater in an alluvial aquifer system in the Sultanate of Oman: Hydrogeology Journal, v. 14, p. 203–224.

Mattey, D.P., Fairchild, I.J., and Atkinson, T.C., 2009, Seasonal microclimate control on calcite fabrics, stable isotopes and trace elements in modern speleothem from St. Michaels Cave, Gibraltar: Geochimica et Cosmochimica Acta, v. 73, p. A849.

McMillan, E., Fairchild, I., Frisia, S., Borsato, A., and McDermott, F., 2005, Annual trace element cycles in calcite–aragonite speleothems: evidence of drought in the western Mediterranean 1200–1100 yr BP: Journal of Quaternary Science, v. 20, p. 423–433.

Mervine, E.M., Humphris, S.E., Sims, K.W.W., Kelemen, P.B., and Jenkins, W.J., 2014, Carbonation rates of peridotite in the Samail Ophiolite, Sultanate of Oman, constrained through ^{14}C dating and stable isotopes: Geochimica et Cosmochimica Acta, v. 126, p. 371–397.

Mickler, P.J., Stern, L.A., and Banner, J.L., 2006, Large kinetic isotope effects in modern speleothems: Geological Society of America, Bulletin, v. 118, p. 65–81.

Monnin, C., Chavagnac, V., Boulart, C., Ménez, B., Gérard, M., Gérard, E., Pisapia, C., Quéméneur, M., Erauso, G., Postec, A., Quentas-Dombrowski, L., Payri, C., and Pelletier, B., 2014, Fluid chemistry of the low temperature hyperalkaline hydrothermal system of Prony Bay (New Caledonia): Biogeosciences, v. 11, p. 5687–5706.

Neal, C., and Stanger, G., 1983, Hydrogen generation from mantle source rocks in Oman: Earth and Planetary Science Letters, v. 66, p. 315–320.

Neal, C., and Stanger, G., 1984, Calcium and magnesium hydroxide precipitation from alkaline groundwaters in Oman, and their significance to the process of serpentinization: Mineralogical Magazine, v. 48, p. 237–241.

O'Neil, J.R., and Barnes, I., 1971, C^{13} and O^{18} compositions in some fresh-water carbonates associated with ultramafic rocks and serpentinites: western United States: Geochimica et Cosmochimica Acta, v. 35, p. 687–697.

Pallister, J., and Hopson, C., 1981, Samail ophiolite plutonic suite: field relations, phase variation, cryptic variation and layering, and a model of a spreading ridge magma chamber: Journal of Geophysical Research, v. 86, p. 2593–2644.

Pauckert, A.N., Matter, J.M., Kelemen, P.B., Shock, E.L., and Havig, J.R., 2012, Reaction path modeling of enhanced in situ CO_2 mineralization for carbon sequestration in the peridotite of the Samail Ophiolite, Sultanate of Oman: Chemical Geology, v. 330–331, p. 86–100.

Pentecost, A., 2005, Travertine: Berlin, Springer-Verlag, 445 p.

Pentecost, A., and Viles, H., 1994, A review and reassessment of travertine classification: Géographie Physique et Quaternaire, v. 48, p. 305–314.

Pola, M., Gandin, A., Tuccimel, P., Soligo, M., Deiana, R., Fabbri, P., and Zampieri, D., 2014, A multidisciplinary approach to understanding carbonate deposition under tectonically controlled hydrothermal circulation: a case study from a recent travertine mound in the Euganean hydrothermal system, northern Italy: Sedimentology, v. 61, p. 172–199.

Python, M., and Ceuleneer, G., 2003, Nature and distribution of dykes and related melt migration structures in the mantle section of the Oman ophiolite: Geochemistry Geophysics Geosystems, v. 4, p. 1–34.

Renaut, R.W., and Jones, B., 1997, Controls on aragonite and calcite precipitation in hot spring travertines at Chemurkeu, Lake Bogoria, Kenya: Canadian Journal of Earth Sciences, v. 34, p. 801–818.

Sader, J.A., Leybourne, M.I., McClenaghan, M.B., and Hamilton, S.M., 2007, Low-temperature serpentinization processes and kimberlite groundwater signatures in the Kirkland Lake and Lake Timiskiming kimberlite fields, Ontario, Canada: implications for diamond exploration: Geochemistry: Exploration, Environnement, Analysis, v. 7, p. 3–21.

Sano, Y., Urabe, A., Wakita, H., and Wushiki, H., 1992, Origin of hydrogen–nitrogen gas seeps, Oman: Applied Geochemistry, v. 8, p. 1–8.

Schwarzenbach, E.M., Lang, S.Q., Fruh-Green, G.L., Lilley, M.D., Bernasconi, S., and Méhay, S., 2013, Sources and cycling of carbon in continental, serpentinite-hosted alkaline springs in the Voltri Massif, Italy: Lithos, v. 177, p. 236–244.

Sinclair, D.J., 2011, Two mathematical models of Mg and Sr partitioning into solution during incongruent calcite dissolution: Chemical Geology, v. 283, p. 119–133.

Sinclair, D.J., Banner, J.L., Taylor, F.W., Partin, J., Jenson, J., Mylroie, J., Goddard, E., Quinn, T., Jocson, J., and Miklavič, B., 2012, Magnesium and strontium systematics in tropical speleothems from the Western Pacific: Chemical Geology, v. 294–295, p. 1–17.

Teboul, P.A., Durlet, C., Gaucher, E.C., Virgone, A., Girard, J.-P., Curie, J., Lopez, B., and Camoin, G.F., 2016, Origins of elements building travertine and tufa: new perspective provided by isotopic and geochemical tracers: Sedimentary Geology, v. 334, p. 97–114.

Van der Lee, J., 1998, Thermodynamic and mathematical concepts of CHESS: technical report LHM/RD/98/3, Ecole des Mines de Paris, Centre d'Informatique Géologique, Fontainebleau, France.

Veysey, J., Fouke, B., Kandianis, M., Schickel, T., Johnson, R., and Goldenfeld, N., 2008, Recontruction of water temperature, pH, and flux of ancient hot springs from travertine depositional facies: Journal of Sedimentary Research, v. 78, p. 69–76.

Weyhenmeyer, C.E., 2000, Origin and Evolution of Groundwater in the Alluvial Aquifer of the Eastern Batinah Coastal Plain, Sultante of Oman [Ph.D. Thesis]: Universität Bern, 202 p.

Weyhenmeyer, C.E., Burns, S.J., Waber, H.N., Aeschbach-Hertig, W., Kipfer, R., Loosli, H.H., and Matter, A., 2000, Cool glacial temperatures and changes in moisture source recorded in Oman groundwaters: Science, v. 287, p. 842–845.

Weyhenmeyer, C.E., Burns, S.J., Waber, H.N., Macumber, P.G., and Matter, A., 2002, Isotope study of moisture sources, recharge areas, and groundwater flow paths within the eastern Batinah coastal plain, Sultanate of Oman: isotopes study of groundwater movement in Oman: Water Resources Research, v. 38, p. 1–22.

Received 10 February 2015; accepted 26 September 2016.